Evaluation of Thermal Resistance of Surface-emitting Quantum Cascade Laser using Structural Function and 3D Thermal Flow Simulation

Shigeyuki Takagi[1], Hirotaka Tanimura[1][a], Tsutomu Kakuno[2], Rei Hashimoto[2], Kei Kaneko[2] and Shinji Saito[2]

[1]*Department of Electrical and Electronics Engineering, School of Engineering, Tokyo University of Technology, 1404-1 Katakura-cho, Hachioji, Tokyo, Japan*
[2]*Corporate Manufacturing Engineering Center, Toshiba Corporation, 8 Shinisogo-cho, Isogo, Yokohama, Kanagawa, Japan*

Abstract: We analysed the thermal characteristics of a surface-emitting quantum cascade laser (QCL), which is expected to increase output and improve beam quality, on the basis of structural functions and 3D thermal flow simulation. The surface-emitting QCL has a device size of 3 mm x 3 mm and has a photonic crystal for extracting laser light vertically from the QCL. The structural function indicating the heat capacity and thermal resistance of the surface-emitting QCL was measured by the static method, and the total thermal resistance including the mount was about 4.7 K/W. On the other hand, the thermal resistance calculated from the 3D thermal flow simulation of the surface-emitting QCL was 4.55 K/W, showing the results of the two methods to be in good agreement. It was shown that the structural function and the 3D simulation are effective for the thermal analysis of surface-emitting QCLs.

1 INTRODUCTION

Quantum cascade lasers (QCLs) are n-type semiconductor lasers that can emit laser light in the infrared region (Faist et al., 1994). Since the oscillation wavelength of the QCL is in the infrared region called the fingerprint region of molecules, many gases can be measured with high sensitivity. In particular, QCLs are applicable to trace substance detection and distant gas detection. With such trace substance detection and distant gas detection, higher sensitivity is expected upon increasing the output. Since the amount of laser absorption is measured in the detection of trace substances, it is necessary to propagate a large optical path length. Also, in far-field gas detection, a high-power laser is required since the weakly reflected light during laser light propagation is detected.

Regarding high-power lasers, watt-class laser oscillation has been reported by Evans et al. (Evans et al., 2007). This laser is an end-face emitting-type laser in which the directions of the laser excitation and the laser emission coincide with each other. In an end-face light-emitting laser, the laser beam is excited by concentrating the current along a narrow current path called a ridge, and heat dissipation is low. Moreover, the laser beam is emitted from the narrow ridge into a wide space, and the rapid expansion of the beam area causes the deterioration of the beam quality.

On the other hand, a surface-emitting QCL that emits laser light in the vertical direction of the device using a photonic crystal (PhC) has been proposed. By increasing the area of the excited part called a mesa, improvements of the beam quality and the heat dissipation can be expected. In the surface emitting QCL using PhC, laser oscillation was reported by Colombelli et al. (Colombelli et al., 2003), and laser oscillation of 5 W was reported by Wang et al. (Wang et al., 2019).

[a] https://orcid.org/0000-0002-7653-4602

It has been reported that the gain of QCLs improves with decreasing temperature (Gresch et al., 2009). Therefore, it is important to improve the cooling of the device, that is, the heat dissipation of the device in order to increase the laser power. Since thermal resistance is the ratio of temperature rise to power input, in this paper we use thermal resistance as an index of heat dissipation. By reducing the thermal resistance, high heat dissipation can be achieved and the laser output power can be improved.

We have reported on the relationship between the ridge structure and the heat-dissipating structure using structural functions and simulations in an end-face light-emitting QCL (Takagi et al., 2019). Laser oscillations of the surface-emission type QCLs have been reported, but there are few reports on their thermal analysis.

So far, we have reported the results of applying the structural functions and the thermal simulations to the thermal analysis of end-face emission QCLs. The structural function was measured by applying the static method to the surface-emitting QCL, and the thermal resistance of the device was extracted to be about 4.7 K/W. On the other hand, thermal analysis was performed using a 3D simulation model for the surface emitting QCL, and a thermal resistance of 4.55 K/W was obtained. The thermal resistance values obtained by the two methods were in good agreement. It has been shown that both methods are effective for the thermal analysis of surface-emitting QCLs.

2 SURFACE-EMITTING QCL

The structure of the surface-emitting QCL is shown in Fig. 1, where (a) is a cross-sectional view, (b) is a top view, and (c) is a bottom view. A mesa area that emits laser light and a dummy ridge are formed on an InP substrate of 600 µm thickness. In the mesa area, InP layer is formed on the active layer that excites the laser, a photonic crystal made of InGaAs is formed on the InP layer, and the photonic crystal is embedded with AuSn. An Au electrode for current supply is formed on the opposite side of the InP substrate. The surface-emitting device has an epi-side-down structure in which the mesa and dummy ridge sides are mounted on a Cu/W mount with AuSn solder.

Figure 2 shows a photograph of the surface-emitting QCL used for the measurement, in which the mesa and dummy ridge are observed to be formed on the InP substrate.
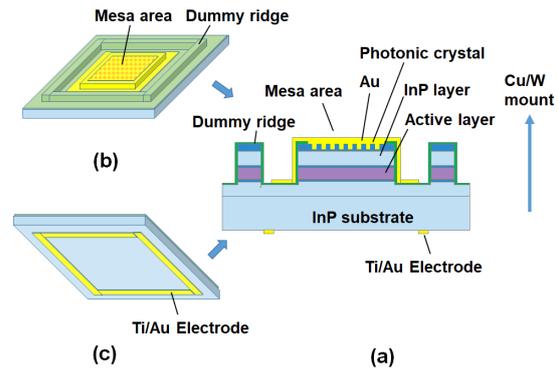

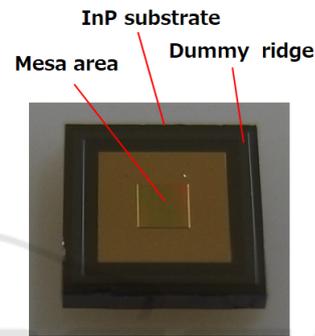Figure 1: Surface emitting QCL. (a) Cross-sectional view, (b) top view, and (c) bottom view.

Figure 2: Photograph of surface-emitting QCL.

3 MEASUREMENT OF STRUCTURE FUNCTION

3.1 K-factor Measurement

Dynamic and static methods are used to measure the thermal resistance of semiconductor devices. The static method is a method of measuring the thermal resistance from the voltage/current characteristics at the time of cooling after heating the device. The measurement time is short and the reproducibility is excellent (Székely, 1997).

We have reported a method for measuring the thermal resistance of an end-face emitting QCL by the static method. In this study, we applied a static method to the thermal resistance measurement of the surface-emitting QCL. The T3Ster (Siemens AG) shown in Fig. 3 was used for the measurement. Since the total thermal resistance of a semiconductor device changes with temperature, the temperature change is proportional to the voltage change at the end of the device when a constant current is flowing. In the static method, the voltage change of ΔTSP [mV] is

measured, and the device temperature change of ΔT_j [K] is calculated using

$$\Delta T_j = K \cdot \Delta TSP \ , \tag{1}$$

where K is a coefficient called the K-factor.

The K-factor is required to measure the temperature of a surface-emitting QCL by the static method. The surface-emitting QCL was installed in the thermostat shown in Fig. 3. The thermostat temperature was changed from 20 °C to 70 °C, and the K-factor was measured. Figure 4 shows the measurement result of the K-factor of the surface-emission QCL. As a result, the K-factor of –0.02243 V/° was obtained.
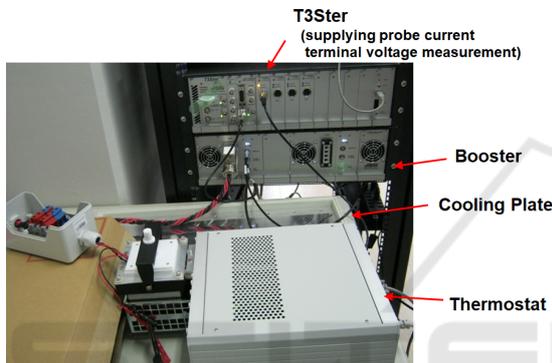

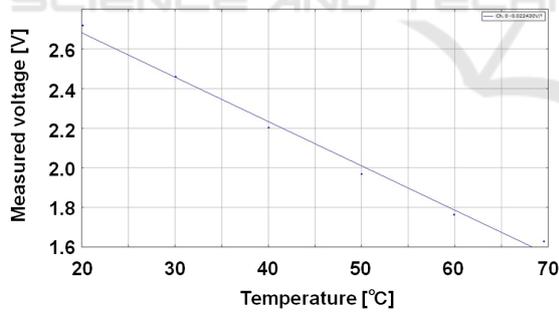Figure 3: Measuring Equipment of K-factor and structure function.

Figure 4: Measurement result of K-factor.

3.2 Measurement of Structure Function

T3Ster was also used to measure the structural function by the static method. The QCL mount was set on the cooling plate of T3Ster. The QCL mount was cooled to 20 °C, and the QCL device was heated by supplying about 200 mA of electric current. After stopping the heating power supply, the QCL temperature during cooling was measured and the

cooling curve was obtained. Denoting the thermal resistance as R_{th} and the thermal capacity as C_{th} in the elements constituting the QCL, the time constant τ during cooling is expressed by

$$\tau = C_{th} \cdot R_{th} \ . \tag{2}$$

The time constant τ was extracted from the inflection point of the cooling curve, and C_{th} and R_{th} were obtained from τ using Eq. (2). In structural functions graphs, R_{th} is plotted on the horizontal axis and C_{th} is plotted on the vertical axis (Székely, 1997).

Figure. 5 shows the structural function of the surface-emitting QCL. As shown in Fig. 1, the surface-emitting QCL is divided into the mount, AuSn solder, PhC, InP layer, and the active layer. From the thermal conductivity and component size, it is estimated that the structural function divided by inflection points corresponds to the four QCL components. In addition, the flat region with a thermal resistance of 5 K/W or more changes depending on whether the QCL is attached to a cooling plate and is considered to be the thermal resistance between the surface-emitting QCL and the T3Ster cooling plate. The total thermal resistance of the surface emitting QCL is estimated to be about 4.7 K/W.
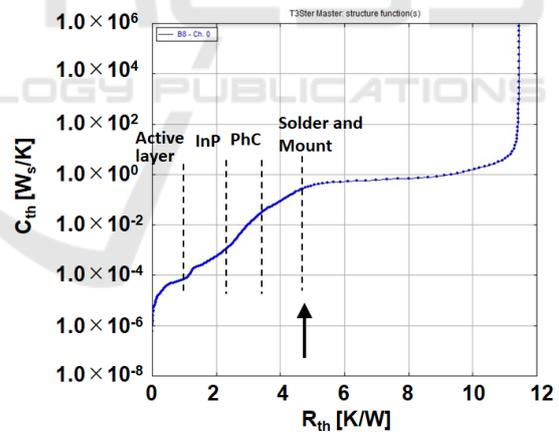

Figure 5: Measurement results of structure function.

4 THERMAL SIMULATION OF SURFACE-EMITTING QCL

4.1 3D Thermal Flow Simulation Model

As another method for analysing the thermal characteristics of the surface-emitting QCL, thermal

flow simulation using a 3D model was performed. The 3D configuration and physical property data of the surface-emitting QCL were input to the simulation model. The thermal flow simulation software FloTHERM (Siemens Product Lifecycle Management Software Inc.) was used for the simulator. The simulation is performed using a natural convection model in which the active is overheated and natural convection is generated (Ho et al., 2008). The equation for gas flow is expressed by

$$\frac{\partial \rho}{\partial t} + \frac{\partial(\rho v_x)}{\partial x} + \frac{\partial(\rho v_y)}{\partial y} + \frac{\partial(\rho v_z)}{\partial z} = 0, \quad (3)$$

where ρ is density, t is time, and v_x, v_y, and v_z are velocities in the x, y, and z directions, respectively. The heat equation is determined as

$$\frac{\partial u}{\partial t} = \frac{K}{\sigma \rho}\left(\frac{\partial^2 u}{\partial x^2} + \frac{\partial^2 u}{\partial y^2} + \frac{\partial^2 u}{\partial z^2}\right) + \frac{1}{\sigma} F(x, y, z, t), \quad (4)$$

where u is the temperature and is a function of the position and time. σ is the specific heat, and K is the thermal conductivity. F is the external heating value per time, and is a function of position and time.

Figure 6 (a) shows the three-dimensional model of the surface-emitting QCL. The InP substrate with the mesa area on the lower side is placed on the Cu/W mount, and the mount is fixed on the Peltier element. Figure 6 (b) shows the top view of the 3D model as shown in Fig. 2. The outlines of the InP substrate, AuSn solder, mesa, dummy ridge, and the Au electrode on the opposite side of the InP substrate to the mesa are observed.
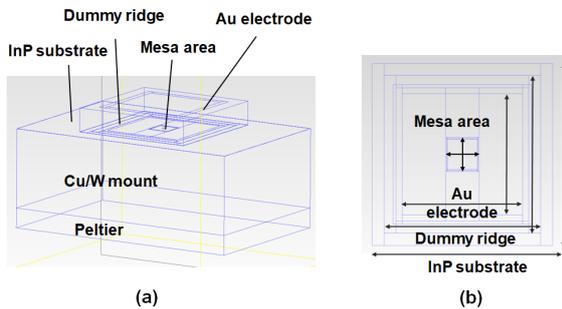

Figure 5: 3D thermal flow model (a) and its top view.

In the 3D model, the temperature distributions in the QCL components were simulated using the isotropic thermal conductivities as follows. The thermal conductivity of the Cu/W mount, AuSn solder, InP, SiO$_2$, Ti, Au, and Cu are 157 W/mK, 59 W/ mK, 68 W/mK, 1.38 W/mK, 21 W/mK, 296 W/mK, and 403 W/mK, respectively. For the PhC in which Au was embedded, the thermal conductivity was calculated using the volume ratio of PhC and Au. In the active layer, thin films of Al$_{0.638}$In$_{0.362}$As and Ga$_{0.331}$In$_{0.669}$As were alternately laminated. The thermal conductivity of the active layer was calculated by multiplying the film thickness ratio with InAlAs of 10.0 W/mK (Kim et al., 2002) and InGaAs of 5.6 W/mK (Adachi, 1985), and was estimated to be 7.5 W/ mK.

The temperature boundary condition is fixed at 0 °C on the mount with a cooling Peltier device, and the ambient temperature of the surface-emitting QCL is set at 30 °C. Assuming that the power from the power supply is input to the active layer, the temperature rise was calculated by changing the power supplied to the active layer.

4.2 Simulation Results

The temperature distribution of the surface-emitting QCL was calculated by changing the input power to the active layer to 2 and 10 W. Figures 7 (a) and 7 (b) show the temperature distribution of the surface-emitting QCL in the central cross section. The Cu/W mount has high thermal conductivity, and the temperature in the mount is approximately 0 °C. The temperature is high in the active layer where power is applied and in the mesas around it. The maximum temperature of air is 21.3 °C because the calculation region is set to the region where the temperature of air is affected by the temperature of the surface-emission QCL.

When the input power was increased from 2 to 6 W, as shown in Figs. 7 (a) and (b), the temperature of the mesa area increased from 8.6 to 45.5 °C. Then, the input power to the active layer was increased from 0 W to 16 W, and the relationship between the input power to the active layer and the maximum temperature of the surface-emission QCL was calculated. The simulation results are shown in Fig. 8. The maximum temperature of the surface emitting QCL increases in proportionally to the power input to the active layer. Figure 8 shows that the maximum temperature rise at 10 W is 45.5 °C (K), and the thermal resistance is estimated to be 4.55 K/W.
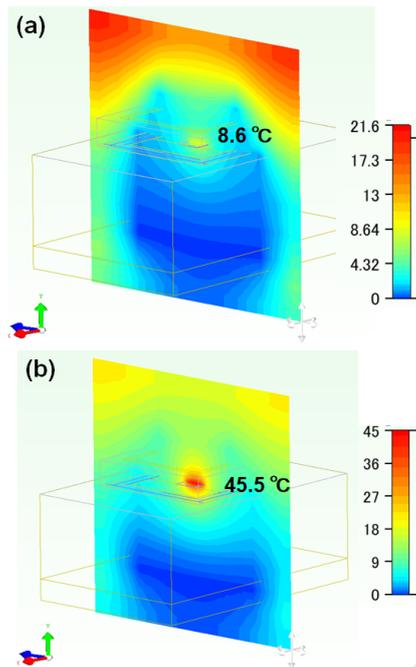
Figure 6: Simulation results of thermal flow analysis. (a) Input power: 2 W, (b) Input power: 10 W.
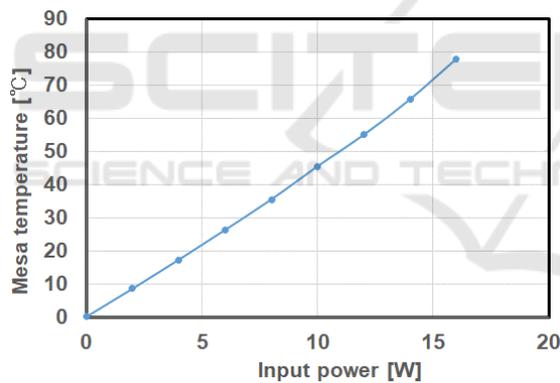

Figure 7: Relationship between input power and maximum temperature of the mesa section.

5 DISCUSSION AND CONCLUSIONS

In the surface-emitting QCL, the Cu/W mount with the size of 6 x 4 x 2 (t) mm has the maximum heat capacity of the device. The heat capacity is calculated to be 0.123 J/K from the density of 17.2 g/cm^3 and the specific heat of 0.15 kJ/(kg/K). This is almost the same as the thermal resistance of the threshold value at which the heat capacity becomes flat in the structural function. Therefore, it is reasonable to

estimate the thermal resistance of the structural function to be about 4.7 K/W.

On the other hand, the thermal resistance is calculated to be 4.55 K/W from the 3D simulation, and the thermal resistances obtained by 3D simulation are in good agreement with that obtained from the structure function. Therefore, the thermal analyses using the structural function and 3D simulation are effective for calculating the thermal characteristics of the surface-emitting QCL. In addition, thermal resistance measurement using the structural function is effective for evaluating the validity of the calculation model of 3D simulation.

ACKNOWLEDGMENTS

REFERENCES

Faist, J., Capasso, F., Sivco, D. L., Sirtori, C., Hutchinson, A., & Cho, A. Y. (1994). Quantum cascade laser. *Science*, 264, 553-556.

Evans, A., Darvish, S. R., Slivken, S., Nguyen, J., Bai, Y., & Razeghi, M. (2007). Buried heterostructure quantum cascade lasers with high continuous-wave wall plug efficiency. *Appl. Phys. Lett.*, 91, 071101-1-3.

Colombelli, R., Srinivasan, K., Troccoli, M., Painter, O., Gmachl, C. F., Tennant, D. F., Sergent, A. M., Sivco, D. L., Cho, A. Y., & Capasso, F. (2003). Quantum cascade surface-emitting photonic crystal laser. *Science*, 302, 1374–1377.

Wang, Z., Liang., Y., Meng, B., Sun., Y-T., Omanakttan, G., Gini, E., Beck, M., Ilia, S., Lourdudoss, S., Faist, J., Scalari, G. (2019). Large area photonic crystal quantum cascade laser with 5 W surface-emitting power. *Opt. Express*, 27, 22708–22716.

Gresch, T., Faist, J., & Giovannini, M. (2009). Gain measurements in strain-compensated quantum cascade laser. *Appl. Phys. Lett.*, 94, 161114-1-3.

Takagi, S., Tanimura, H., Kakuno, T., Hashimoto, R., Saito, S. (2019). Thermal analysis and heat dissipation improvement for quantum cascade lasers through experiments, simulations, and structure function. *Jpn. J. Appl. Phys.*, 58, 091008-1–6.

Székely, V. (1997). A new evaluation method of thermal transient measurement results. *Microelectron. J.*, 28, 277–292.

Ho, C. J., Chen, M. W., Li, Z. W. (2008). Numerical simulation of natural convection of nanofluid in a square enclosure: Effects due to uncertainties of viscosity and thermal conductivity. *Int. J. Heat Mass Transfer*, 51, 4506–4515.

Kim, Y. M., Rodwell, M. J. W., Gossard, A. C. (2002). Thermal characteristics of InP, InAlAs, and AlGaAsSb metamorphic buffer layers used in In0.52Al0.48/In0.53Ga0.47As heterojunction bipolar transistors grown on GaAs substrates. *J. Electron. Mater.*, 31, 196–199.

Adachi, S. (1985). GaAs, AlAs, and AlxGa1−xAs: Material parameters for use in research and device applications. *J. Appl. Phys.*, 58, R1–R29.